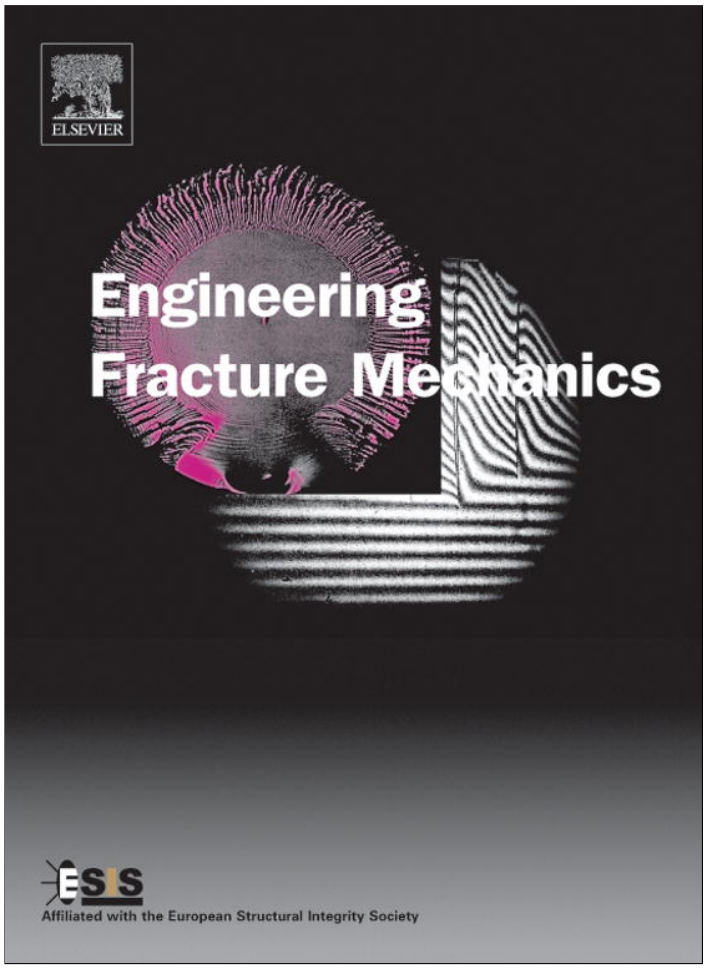

(This is a sample cover image for this issue. The actual cover is not yet available at this time.)

Engineering Fracture Mechanics 97 (2013) 216–226

Contents lists available at SciVerse ScienceDirect

Engineering Fracture Mechanics

journal homepage: www.elsevier.com/locate/engfracmech

A Finite Fracture Mechanics approach to V-notched elements subjected to mixed-mode loading

Alberto Sapora *, Pietro Cornetti, Alberto Carpinteri

Department of Structural, Building and Geotechnical Engineering, Politecnico di Torino, Corso Duca degli Abruzzi 24, 10129 Torino, Italy

ARTICLE INFO

Article history:
Received 28 February 2012
Received in revised form 9 November 2012
Accepted 12 November 2012
Available online 23 November 2012

Keywords:
Brittle V-notched elements
Mixed mode loading
Finite Fracture Mechanics

ABSTRACT

The coupled Finite Fracture Mechanics (FFM) criterion is applied to investigate the mixed mode fracture initiation in V-notched brittle elements. The analysis involves the determination of the crack propagation angle and of the critical value of the generalized stress intensity factor (SIF), which are supposed to be the governing failure parameters within brittle structural behavior. The criterion is validated by comparing its predictions with experimental data available in the literature and with results by other approaches based on a critical distance.

1. Introduction

Different criteria have been proposed to deal with fracture initiation of V-notched elements under mode I loading conditions, by evaluating either the stress [1–4] or energy-related quantities [5–8] over a distance Δ from the notch tip and by comparing them with a function of either the tensile strength σ_u or the fracture toughness K_{Ic}. Accordingly, the length Δ results a material constant.

On the other hand, all the above criteria present some drawbacks [9] and, in order to overcome them, two coupled stress and energy approaches have been proposed: Leguillon's criterion [10] and FFM [9,11]. They are based on the same discrete energy balance, but while the former also considers a point-wise stress condition, the latter involves in addition the satisfaction of an average stress requirement. Accordingly, the internal length Δ becomes a structural parameter, thus able to take into account the interaction between the finite crack advance and the geometry of interest. The accuracy of the failure load predictions related to notched structures has shown the great potentiality of the coupled criteria, both for what concerns sharp V-notches [7,12] and blunted V-notches [13–16]. Indeed, FFM was generally found to provide the best results [12,15].

The investigation of fracture initiation in V-notched brittle elements loaded under mixed mode (mode I + mode II) is more complex. It involves the determination of both the failure load and the crack propagation angle. Close estimations on the former are usually obtained by different criteria [17–19], so that a best approach cannot be univocally defined just on this basis [20,21]. On the other hand, significant differences of predictions are generally observed for the latter. In [20] it has been shown that the maximum circumferential stress criterion [2] and the average stress criterion [18] furnish good results, while the strain energy density criterion [17] reveals to be less accurate. The generalization of this approach proposed in [21,22] is not able to estimate the critical angle. Eventually, Yosibash–Leguillon criterion, which represents the extension of Leguillon's criterion to mixed mode, was found to provide accurate results, although they were obtained with an accuracy of five degrees [21].

* Corresponding author.
E-mail addresses: alberto.sapora@polito.it (A. Sapora), pietro.cornetti@polito.it (P. Cornetti), alberto.carpinteri@polito.it (A. Carpinteri).

0013-7944/$ - see front matter © 2012 Elsevier Ltd. All rights reserved.
http://dx.doi.org/10.1016/j.engfracmech.2012.11.006

Nomenclature

c	length of a crack stemming from the notch tip
E	Young's modulus
F_c	critical failure load
G	crack driving force
G_c	fracture energy
K_{I}	mode I stress intensity factor
K_{II}	mode II stress intensity factor
K_{Ic}	fracture toughness
K^*_{I}	mode I generalized stress intensity factor
K^*_{II}	mode II generalized stress intensity factor
K^*_{Ic}	generalized fracture toughness
K^*_{If}	critical value of the mode I generalized stress intensity factor in mixed-mode fracture
$\bar{m}$	dimensionless mode mixity
θ	crack propagation angle
θ_c	critical crack propagation angle
λ_{I}	mode I Williams' eingenvalues
λ_{II}	mode II Williams' eingenvalues
ρ	notch root radius
$\bar{\rho}$	dimensionless root radius
σ_u	tensile strength
ω	notch amplitude
Δ	finite crack advance
Δ_c	critical finite crack advance

In the present paper, the above problem is addressed by means of FFM as it provides promising results for the case of mode I loading conditions. The expressions for the critical crack advance and the generalized fracture toughness, both depending on the propagation angle, are firstly derived. The study involves the characterization of the stress field and of the crack driving force in proximity of the notch tip: while the former is known analytically [23], discrete values for the latter are presented in the literature [19,24]. Finite Fracture Mechanics is then applied to a large variety of experimental results [19,21,22,25], in order to investigate a wide range of mode mixity ratios [26]. Predictions by the average stress criterion [18] and Yosibash–Leguillon approach [19] are also considered, for the sake of completeness.

2. Coupled FFM criterion

According to the coupled FFM criterion [9,11], fracture is supposed not to propagate continuously, but by finite crack extensions, whose value is determined by the contemporaneous fulfilment of a stress requirement (Section 2.1) and an energy balance (Section 2.2). By coupling these two conditions at incipient failure, the crack propagation angle and the generalized fracture toughness can be derived (Section 2.3).

Notice that the dependence of the quantities on the notch amplitude ω (Fig. 1) will be omitted in the following sections, for the sake of simplicity.

2.1. Stress requirement

By referring to the polar coordinate system (r,θ) at the V-notch root presented in Fig. 1, the stress fields $\sigma_{\theta\theta}(r,\theta)$ and $\tau_{r\theta}(r,\theta)$, in the proximity of the notch tip, can be expressed as:

$$\sigma_{\theta\theta}(r,\theta)=\frac{K^*_{\mathrm{I}}}{(2\pi r)^{1-\lambda_{\mathrm{I}}}}f^{\mathrm{I}}_{\theta\theta}(\theta)+\frac{K^*_{\mathrm{II}}}{(2\pi r)^{1-\lambda_{\mathrm{II}}}}f^{\mathrm{II}}_{\theta\theta}(\theta), \tag{1}$$

and

$$\tau_{r\theta}(r,\theta)=\frac{K^*_{\mathrm{I}}}{(2\pi r)^{1-\lambda_{\mathrm{I}}}}f^{\mathrm{I}}_{r\theta}(\theta)+\frac{K^*_{\mathrm{II}}}{(2\pi r)^{1-\lambda_{\mathrm{II}}}}f^{\mathrm{II}}_{r\theta}(\theta), \tag{2}$$

where $(K^*_{\mathrm{I}},K^*_{\mathrm{II}})$ are the generalized SIFs [27] and $(\lambda_{\mathrm{I}},\lambda_{\mathrm{II}})$ are the Williams' eigenvalues, for mode I (symmetrical) and mode II (anti-symmetrical) loading conditions, respectively. The functions $f_{\theta\theta}$ and $f_{r\theta}$ are provided in the Appendix [23].

The FFM stress condition requires that the average stress $\sigma_{\theta\theta}(r,\theta)$ upon the crack advance Δ is higher than material tensile strength σ_u:

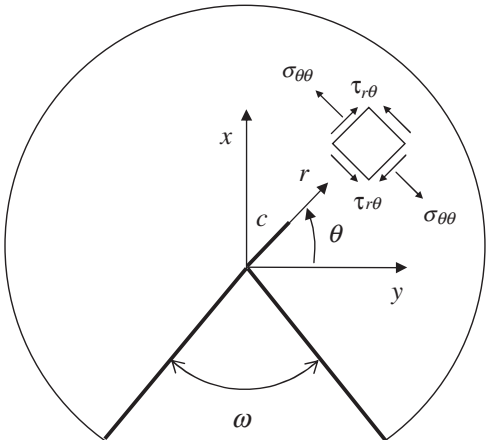

Fig. 1. V-notch with Cartesian and Polar coordinate systems and crack of length c emanating from the notch tip.

$$\int_0^{\Delta} \sigma_{\theta\theta}(r,\theta)\mathrm{d}r \geqslant \sigma_u \Delta. \tag{3}$$

Substituting Eq. (1) into Eq. (3) and integrating, yields:

$$\frac{K_{\mathrm{I}}^*}{\Delta^{1-\lambda_{\mathrm{I}}}}\bar{f}_{\theta\theta}^{\mathrm{I}}(\theta)+\frac{K^*{}_{\mathrm{II}}}{\Delta^{1-\lambda_{\mathrm{II}}}}\bar{f}_{\theta\theta}^{\mathrm{II}}(\theta) \geqslant \sigma_u, \tag{4}$$

where

$$\bar{f}_{\theta\theta}^{\mathrm{I}}(\theta)=\frac{f_{\theta\theta}^{\mathrm{I}}(\theta)}{\lambda_{\mathrm{I}}(2\pi)^{1-\lambda_{\mathrm{I}}}}, \qquad \bar{f}_{\theta\theta}^{\mathrm{II}}(\theta)=\frac{f_{\theta\theta}^{\mathrm{II}}(\theta)}{\lambda_{\mathrm{II}}(2\pi)^{1-\lambda_{\mathrm{II}}}}. \tag{5}$$

2.2. Energy balance

The FFM energy balance ensures that the energy available for a crack increment Δ (obtained by integrating the crack driving force $G(c,\theta)$ over Δ) is higher than the energy necessary to create the new fracture surface $G_c\Delta$:

$$\int_0^{\Delta} G(c,\theta)\mathrm{d}c \geqslant G_c\Delta. \tag{6}$$

By means of the well-known Irwin's relationship, the crack driving force under plane strain conditions can be expressed as:

$$G(c,\theta)=\frac{K_{\mathrm{I}}^2(c,\theta)}{E'}+\frac{K_{\mathrm{II}}^2(c,\theta)}{E'} \tag{7}$$

where $(K_{\mathrm{I}},K_{\mathrm{II}})$ are the mode I and mode II SIFs, respectively, and $E'=E/(1-\nu^2)$, E being the Young's modulus and ν the Poisson's ratio of the material. The SIFs for a short crack of length c stemming from the notch tip at an angle θ (Fig. 1) can be obtained, starting from the approximate analytical weight functions g presented in [24], by a suitable application of the principle of effects superposition. In fact, provided that $c \ll d$, d being the notch depth, through Eqs. (1) and (2), K_{I} reads:

$$\begin{aligned} K_{\mathrm{I}}(c,\theta) &= \int_0^c \frac{1}{\sqrt{c}}\left[g_\sigma^{\mathrm{I}}(r/c,\theta)\cdot\sigma_{\theta\theta}(r,\theta)+g_\tau^{\mathrm{I}}(r/c,\theta)\cdot\tau_{r\theta}(r,\theta)\right]\mathrm{d}r \\ &= K_{\mathrm{I}}^* c^{\lambda_{\mathrm{I}}-1/2}\int_0^1\left[\frac{g_\sigma^{\mathrm{I}}(t,\theta)f_{\theta\theta}^{\mathrm{I}}(\theta)+g_\tau^{\mathrm{I}}(t,\theta)f_{r\theta}^{\mathrm{I}}(\theta)}{(2\pi t)^{1-\lambda_{\mathrm{I}}}}\right]\mathrm{d}t+K_{\mathrm{II}}^* c^{\lambda_{\mathrm{II}}-1/2}\int_0^1\left[\frac{g_\sigma^{\mathrm{I}}(t,\theta)f_{\theta\theta}^{\mathrm{II}}(\theta)+g_\tau^{\mathrm{I}}(t,\theta)f_{r\theta}^{\mathrm{II}}(\theta)}{(2\pi t)^{1-\lambda_{\mathrm{II}}}}\right]\mathrm{d}t \\ &= K_{\mathrm{I}}^* c^{\lambda_{\mathrm{I}}-1/2}\beta_{11}(\theta)+K_{\mathrm{II}}^* c^{\lambda_{\mathrm{II}}-1/2}\beta_{12}(\theta), \end{aligned} \tag{8}$$

while K_{II} writes:

$$K_{II}(c,\theta) = \int_0^c \frac{1}{\sqrt{c}}\left[g_\sigma^{II}(r/c,\theta)\cdot\sigma_{\theta\theta}(r,\theta) + g_\tau^{II}(r/c,\theta)\cdot\tau_{r\theta}(r,\theta)\right]dr$$
$$= K_I^* c^{\lambda_I - 1/2}\int_0^1 \left[\frac{g_\sigma^{II}(t,\theta)f_{\theta\theta}^{I}(\theta) + g_\tau^{II}(t,\theta)f_{r\theta}^{I}(\theta)}{(2\pi t)^{1-\lambda_I}}\right]dt + K_{II}^* c^{\lambda_{II}-1/2}\int_0^1 \left[\frac{g_\sigma^{II}(t,\theta)f_{\theta\theta}^{II}(\theta) + g_\tau^{II}(t,\theta)f_{r\theta}^{II}(\theta)}{(2\pi t)^{1-\lambda_{II}}}\right]dt$$
$$= K_I^* c^{\lambda_I - 1/2}\beta_{21}(\theta) + K_{II}^* c^{\lambda_{II}-1/2}\beta_{22}(\theta). \tag{9}$$

Approximated expressions for the weight function components g in Eqs. (8) and (9) were derived in [24] by a best fit procedure based on numerical results in the range $18^\circ \leqslant \theta \leqslant 90^\circ$ with a step $\theta = 9^\circ$, for $18^\circ \leqslant \omega \leqslant 144^\circ$. The maximum relative error for the SIFs in Eqs. (8) and (9) was estimated in [24] to be lower than 2%, typical errors being less than 1%. Indeed, the same deviation has been observed by comparing the β_{11}-values with those presented in [28,29].

Upon substitution of Eqs. (8) and (9) into Eq. (7) and of the resulting expression into Eq. (6) with $G_c = K_{Ic}^2/E'$, the energy balance can be finally rewritten in the following form:

$$\left(K_I^*\right)^2\bar{\beta}_{11}(\theta)\Delta^{2\lambda_I-1} + K_I^*K_{II}^*\bar{\beta}_{12}(\theta)\Delta^{\lambda_I+\lambda_{II}-1} + \left(K_{II}^*\right)^2\bar{\beta}_{22}(\theta)\Delta^{2\lambda_{II}-1} \geqslant K_{Ic}^2, \tag{10}$$

where

$$\bar{\beta}_{11} = \frac{\beta_{11}^2 + \beta_{21}^2}{2\lambda_I}, \tag{11}$$
$$\bar{\beta}_{12} = 2\frac{\beta_{11}\beta_{12} + \beta_{21}\beta_{22}}{\lambda_I + \lambda_{II}}, \tag{12}$$
$$\bar{\beta}_{22} = \frac{\beta_{12}^2 + \beta_{22}^2}{2\lambda_{II}}. \tag{13}$$

The functions $\bar{\beta}_{11}, \bar{\beta}_{12}$ and $\bar{\beta}_{22}$, for different notch amplitudes over the range $30^\circ \leqslant \theta \leqslant 90^\circ$ with a step $\theta = 5^\circ$, are also tabulated in [19], where they are named H_{11}, $H_{12} + H_{21}$ and H_{22}, respectively. The values have been obtained by means of an asymptotic matching approach: close estimations with those provided by the weight function components g [24] are observed (Fig. 2 refers to the case $\omega = 45^\circ$). Notice that the results shown in [19] must be re-scaled according to the different definition of the generalized SIFs (Eqs. (1) and (2)) and must be divided by $(1 - 0.36^2)$, $\nu = 0.36$ being the Poisson's ratio used in the finite element analysis carried out by the Authors.

2.3. FFM implementation

Before implementing the coupled FFM criterion, let us rewrite Eqs. (4) and (10) in the form:

$$\frac{K_I^*}{\Delta^{1-\lambda_I}}\left[\bar{f}_{\theta\theta}^{I}(\theta) + m(\Delta)\bar{f}_{\theta\theta}^{II}(\theta)\right] \geqslant \sigma_u, \tag{14}$$
$$\left(K_I^*\right)^2\Delta^{2\lambda_I-1}\left[\bar{\beta}_{11}^2(\theta) + m(\Delta)\bar{\beta}_{12}^2(\theta) + m^2(\Delta)\bar{\beta}_{22}^2(\theta)\right] \geqslant K_{Ic}^2, \tag{15}$$

where the following dimensionless parameter m has been introduced:

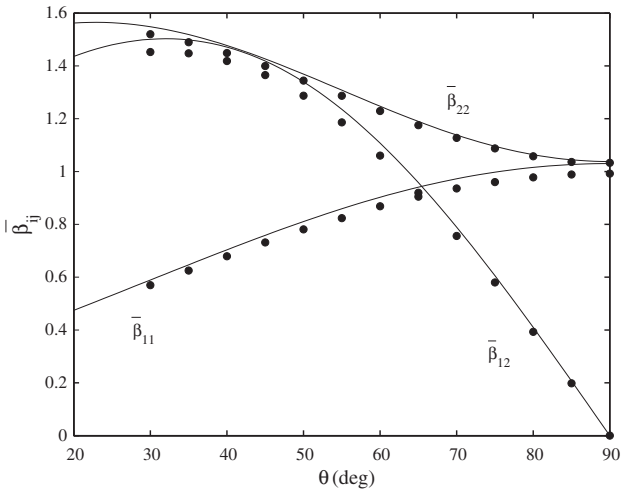

Fig. 2. Functions $\bar{\beta}_{ij}$ for $\omega = 45^\circ$: predictions obtained by using the weight function components g presented in [24] (continuous line) and numerical values reported in [19] (circles).

$$m(\Delta) = \frac{K_{II}^*}{K_I^*}\Delta^{\lambda_{II}-\lambda_I}. \tag{16}$$

Notice that K_I^* is the only quantity in Eqs. (14) and (15) depending on the applied load, m being independent of it (Eq. (16)). Within brittle structural behavior, it can thus be supposed that failure takes place when the mode I generalized SIF reaches the critical value K_{If}^*. At incipient failure, Eqs. (14) and (15) can be grouped into a system of two equations in two unknowns: the critical crack advancement Δ_c and the failure load F_c, implicitly embedded in the function K_{If}^*.

Simple analytical manipulations lead to the following two expressions for Δ_c and K_{If}^*:

$$\Delta_c = \frac{\left[\bar{f}_{\theta\theta}^{I}(\theta_c) + m(\Delta_c)\bar{f}_{\theta\theta}^{II}(\theta_c)\right]^2}{\bar{\beta}_{11}^2(\theta_c) + m(\Delta_c)\bar{\beta}_{12}^2(\theta_c) + m^2(\Delta_c)\bar{\beta}_{22}^2(\theta_c)}\left(\frac{K_{Ic}}{\sigma_u}\right)^2, \tag{17}$$

$$K_{If}^* = \frac{\left[\bar{f}_{\theta\theta}^{I}(\theta_c) + m(\Delta_c)\bar{f}_{\theta\theta}^{II}(\theta_c)\right]^{1-2\lambda_I}}{\left[\bar{\beta}_{11}^2(\theta_c) + m(\Delta_c)\bar{\beta}_{12}^2(\theta_c) + m^2(\Delta_c)\bar{\beta}_{22}^2(\theta_c)\right]^{1-\lambda_I}}\frac{K_{Ic}^{2(1-\lambda_I)}}{\sigma_u^{1-2\lambda_I}}. \tag{18}$$

For a fixed material and a fixed notch amplitude ω, the subsequent procedure is adopted to get the solutions of the coupled Eqs. (17) and (18):

1. Eq. (17) is firstly solved for different θ_c-values, $20° \leqslant \theta_c \leqslant 90°$ with a step $\theta_c = 1°$. A different crack advance Δ_c corresponds to each θ_c. Notice that Eq. (17) represents an implicit equation in the variable Δ_c, since m depends on it (Eq. (16)). In order to overcome this drawback, the *fzero* command of MATLAB® software is utilized: the algorithm uses a combination of bisection, secant and inverse quadratic interpolation methods;
2. each couple (Δ_c,θ_c) obtained at the previous step is then substituted into Eq. (18). The effective critical crack advance Δ_c and the effective crack propagation angle θ_c are those which minimize the K_{If}^* function. Its value can then be exploited to get the critical failure load $F_c \propto K_{If}^*$.

Notice that in the case of pure mode I loading conditions ($m = 0$ and $\theta_c = 90°$), K_{If}^* becomes the generalized fracture toughness K_{Ic}^*. In such a case, Eqs. (17) and (18) revert to the expressions presented in [11].

3. Comparison with experimental data

Finite Fracture Mechanics predictions according to Eqs. (17) and (18) are now compared with experimental results available in the literature. Four data sets are considered, rising from:

- Three-point bending tests on V-notched PMMA samples [19] (Fig. 3a, Section 3.1).
- Four-point bending tests on V-notched MACOR samples [21] (Fig. 3b, Section 3.2).
- Three-point bending tests on V-notched samples made of PMMA at −60 °C [22] (Fig. 3a and c, Section 3.3).
- Arcan tests on double V-notched PMMA samples [25] (Fig. 3d, Section 3.4).

The material properties used in the present analysis are reported in Table 1, while details on the sample geometry can be found tabulated in the quoted references. The eigenvalues λ_I and λ_{II} are plotted in Fig. 4 as functions of the considered notch amplitudes ω.

In the next Sections, predictions by two other theoretical failure criteria will be taken into account, for the sake of completeness. The former is the generalization of Leguillon's criterion [10] to mixed mode by Yosibash and co-workers [19]: it is

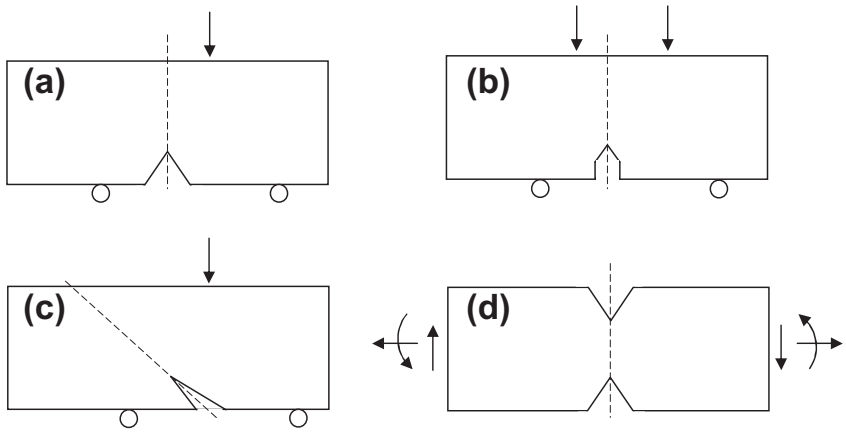

Fig. 3. V-notched samples under different loading conditions.

Table 1
Material properties and dimensionless root radius related to the considered experimental data. Correction factors A refer to mode I loading conditions and depend both on ω and $\bar{\rho}$.

Material properties	PMMA [19]	MACOR [21]	PMMA at −60 °C [22]	PMMA [25]
K_{Ic} (MPa$\sqrt{m}$)	1.12	1.15	1.70	1.20
σ_u (MPa)	111.8	103.0	128.4	102.8
Root radius $\bar{\rho}$	0.299	0.241	0.114–0.382	<0.073
Correction factors A	1.11	1.09	1.04–1.13	<1.03

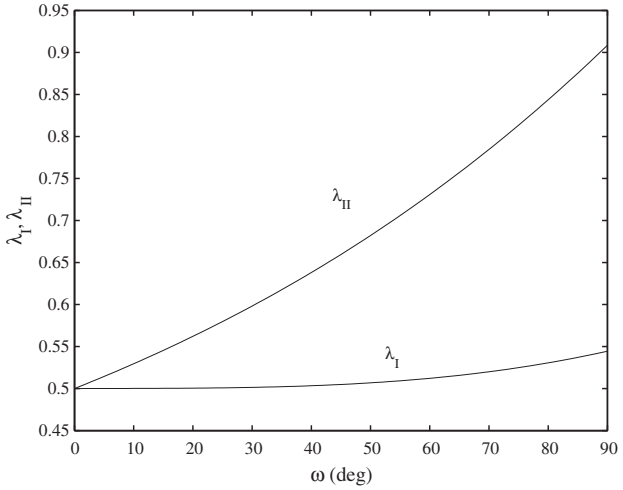

Fig. 4. William's eigenvalues λ_I and λ_{II}, for different notch amplitudes, $0° \leqslant \omega \leqslant 90°$.

similar to FFM, but, differently from Eq. (4), it is based on a point-wise stress condition. This leads to the same coupled Eqs. (17) and (18), with a different definition of the functions $\bar{f}^{I}_{\theta\theta}$ and $\bar{f}^{II}_{\theta\theta}$ (Eq. (5)), namely:

$$\tilde{f}^{I}_{\theta\theta} = \frac{f^{I}_{\theta\theta}(\theta)}{(2\pi)^{1-\lambda_I}}, \qquad \tilde{f}^{II}_{\theta\theta} = \frac{f^{II}_{\theta\theta}(\theta)}{(2\pi)^{1-\lambda_{II}}}. \tag{19}$$

The latter is the average stress criterion proposed in [18]. It is based on the condition (14) with $\Delta_c = 2/\pi \times (K_{Ic}/\sigma_u)^2$, and the corresponding critical value of the generalized SIF writes:

$$K^*_{If} = \frac{(2/\pi)^{1-\lambda_I}}{\left[\bar{f}^{I}_{\theta\theta}(\theta_c) + m(\Delta_c)\bar{f}^{II}_{\theta\theta}(\theta_c)\right]} \frac{K^{2(1-\lambda_I)}_{Ic}}{\sigma^{2\lambda_I-1}_u}. \tag{20}$$

Observe that, in this case, the critical crack advance Δ_c results a material constant: its value was estimated in [1,3] in order to fulfil the extreme situations of crack-free bodies and elements with sufficiently large cracks, see also [11]. On the other hand, Δ_c is expected to vary with the mode-mixity K^*_{II}/K^*_I for what concerns the coupled criteria (Eqs. (16) and (17)). Thus, wanting to render dimensionless the ratio K^*_{II}/K^*_I $\left([L]^{\lambda_I-\lambda_{II}}\right)$, the best choice reveals to be:

$$\bar{m} = \frac{K^*_{II}}{K^*_I}\left(\frac{K_{Ic}}{\sigma_u}\right)^{2(\lambda_{II}-\lambda_I)}. \tag{21}$$

It's important also to outline that all the failure criteria introduced so far refer to a sharp V-notch, i.e. to a notch with a null root radius ρ. On the contrary, since a radius $\rho \neq 0$ was measured in all the tested specimens, this may influence the theoretical predictions. Each data set will be discussed in detail in the incoming analysis, observing that the effect of ρ decreases as:

- the notch amplitude ω increases;
- the dimensionless radius $\bar{\rho} = \rho/(K_{Ic}/\sigma_u)^2$ decreases, i.e. a smaller radius and/or a less brittle material are considered [15];
- the mixity ratio K^*_{II}/K^*_I increases [30].

Table 1 shows the values $\bar{\rho}$ related to the tested samples and the correction factors A to improve the FFM failure load predictions by taking into account the effect of the radius, if elements were subjected to mode I loading conditions [15]. In the present analysis, dealing with mixed mode, the effective correction factors A are expected to be lower than those presented in Table 1, generally justifying the sharpness assumption of the theoretical analysis.

Eventually, notice that the presence of ρ may affect significantly the theoretical predictions on the critical failure load but not those on the propagation angle [30].

3.1. Tests on V-notched PMMA samples

Three point bending tests on V-notched PMMA specimens, with $\omega = 45°$, were carried out in [19]. Mixed mode conditions were obtained by varying both the position of the loading point and of the supports (Fig. 3a). The average experimental results and the theoretical predictions obtained through Eqs. (17)–(20) are shown in Table 2. The estimations by FFM on the crack initiation angle θ_c are in a very good agreement with experimental data, while those on F_c result underestimated of more than 20%. This is partially imputable to the presence of a root radius in the tested samples ($\rho = 30$ μm, Table 1). Although more accurate, FFM predictions considering ρ would always underestimate F_c since correction factors A lower than 1.11 would apply (Table 1). On the other hand, factors A ranging from 1.1 for $\bar{m} = 0.325$ to 1.17 for $\bar{m} = 0.039$ were estimated in [30] by applying Yosibash–Leguillon criterion.

Notice that theoretical predictions by different criteria are very close with each other (Table 2), significant deviations being observed only for higher mixity ratios. The predictions by FFM are always the lowest ones, both for what concerns θ_c and F_c.

Eventually, let us focus our attention on the critical crack advance Δ_c: as $\bar{m}$ increases, Δ_c decreases according to FFM, while it increases according to Yosibash–Leguillon criterion. For the average stress criterion, as observed before, Δ_c results to be a constant, always higher than FFM values.

3.2. Tests on V-notched MACOR samples

Four point-bending MACOR notched specimens, with $\omega = 45°$, were tested in [21]. Mixed mode loading conditions were obtained by varying both the position of the loading points and of the supports (Fig. 3b).

Experimental data and theoretical predictions are reported in Table 3. With the exception of the extreme cases, $\bar{m} = 0.186$ and 1.777, FFM predictions (Eqs. (17) and (18)) on the crack propagation angle show a gap comprised between 8° and 10°.

On the other hand, FFM estimations on the critical failure load are satisfactory, the maximum percentage error being nearly 12% for $\bar{m} = 1.777$. The effect of the notch root radius ($\rho = 30$ μm, Table 1) is less significant than in the previous tests (Section 3.1), mainly because higher mixity ratios are considered [30].

Slightly better results on θ_c are provided by the two other criteria, while the maximum percentage error on F_c is higher: 21% for what concerns Yosibash–Leguillon criterion and nearly 14% for what concerns the average stress approach. These values refer, in both cases, to $\bar{m} = 0.944$.

It can be seen from Table 3 that the trend on the crack advance is the same as that described in Section 3.1: Δ_c-values are a little higher than those presented in Table 2, due to the less brittle material considered.

3.3. Tests on V-notched PMMA at −60 °C samples

Three point bending notched specimens made of PMMA, with different notch amplitudes ($\omega = 30°$, 60° and 90°), were tested at −60 °C in [22]. Both vertical and tilted notches were considered (Fig. 3a and c): the related mixity ratios are shown in Table 4. Notice that, in the present analysis, only the data presented in [22] and referring to the loading position (for vertical notches) and to the support position (for tilted notches) equal to 9 mm have been taken into account. Indeed, the comparison with results related to the other loading/support position leads to conclusions similar to those presented below.

Experimental data and theoretical predictions according to the failure criteria (Eqs. (17)–(20)) are reported in Table 5. The best predictions on θ_c are provided by FFM, although the initiation angles always result overestimated, especially for tilted notches, where deviations greater than 10° are present. On the other hand, dealing with F_c, good results are observed. The maximum deviations refer to the vertical V-notched samples with $\omega = 60°$. This may be due to the measured root radius ($\rho = 67$ μm in Table 4, corresponding to $\bar{\rho} = 0.382$ in Table 1), which results to be the highest one, as the related experimental failure load (Table 5). The influence of ρ is less significant for tilted notches (also because they refer to higher mixity ratios): in this case, Yosibash–Leguillon criterion shows to be the most accurate.

Table 2
Averaged experimental results on PMMA specimens [19], predictions according to FFM, to Yosibash–Leguillon criterion [19] and to the average stress criterion [18].

Experimental values [19]			FFM			Yosibash–Leguillon criterion [19]			Average stress criterion [18]		
$\bar{m}$	θ_c (°)	F_c (N)	θ_c (°)	F_c (N)	Δ_c (μm)	θ_c (°)	F_c (N)	Δ_c (μm)	θ_c (°)	F_c (N)	Δ_c (μm)
0.039	85	226	85	176	61.9	86	178	15.8	86	179	63.9
0.082	79	301	79	222	61.8	81	224	15.9	81	226	63.9
0.114	72	408	75	314	61.7	79	319	16.0	78	320	63.9
0.176	68	613	69	484	61.3	72	494	16.3	72	493	63.9
0.325	60	998	59	759	60.6	61	793	17.2	61	777	63.9

Table 3
Averaged experimental results on MACOR specimens [21], predictions according to FFM, to Yosibash–Leguillon criterion [19] and to the average stress criterion [18].

Experimental values [21]			FFM			Yosibash–Leguillon criterion [19]			Average stress criterion [18]		
$\bar{m}$	θ_c (°)	F_c (kN)	θ_c (°)	F_c (kN)	Δ_c (μm)	θ_c(°)	F_c (kN)	Δ_c (μm)	θ_c(°)	F_c (kN)	Δ_c (μm)
0.186	70	2.20	68	2.10	76.1	71	2.15	20.3	71	2.14	79.4
0.709	52	2.56	44	2.79	73.2	46	3.03	23.9	47	2.88	79.4
0.944	47	3.14	39	3.45	72.1	41	3.79	24.9	43	3.57	79.4
1.200	47	4.55	37	4.12	71.6	37	4.57	25.6	40	4.28	79.4
1.777	34	5.67	33	5.01	70.3	34	5.61	26.6	36	5.23	79.4

Table 4
Mixity ratios and averaged root radius related to experimental tests on V-notched PMMA at −60 °C samples [22]: (v) vertical notches, (t) tilted notches.

ω (°)	30 (v)	60 (v)	90 (v)	30 (t)	60 (t)	90 (t)
$\bar{m}$	0.160	0.100	0.072	1.031	0.679	0.388
ρ (μm)	43	67	20	27	43	22

Table 5
Averaged experimental results on PMMA at −60 °C specimens [22], with both vertical (v) and tilted (t) notches, predictions according to FFM, to Yosibash–Leguillon criterion [19] and to the average stress criterion [18].

Experimental values [22]			FFM			Yosibash–Leguillon criterion [19]			Average stress criterion [18]		
ω (°)	θ_c (°)	F_c (N)	θ_c (°)	F_c (N)	Δ_c (μm)	θ_c (°)	F_c (N)	Δ_c (μm)	θ_c (°)	F_c (N)	Δ_c (μm)
30 (v)	65	896	71	820	108	73	828	27.7	73	834	112
60 (v)	69	1039	77	861	107	80	882	28.7	79	877	112
90 (v)	72	959	80	965	106	83	1024	31.9	82	988	112
30 (t)	24	2228	36	2088	102	37	2235	31.5	40	2172	112
60 (t)	40	3265	46	2881	102	48	3204	36.8	49	2972	112
90 (t)	42	4497	57	4135	101	60	4675	39.3	60	4246	112

3.4. Tests on double V-notched PMMA samples

Double V-notched PMMA specimens, with different notch opening angles $\omega = 20°$, 40°, 60° and 80°, were tested in [25] (Fig. 3d). For each angle, different mixity ratios were obtained by varying the arcan sample inclination. For all the cases, the root radius was very small ($\rho < 10$ μmm), and its effect is not supposed to influence significantly the related results (Table 1).

Experimental results and FFM predictions (Eqs. (17) and (18)) are displayed in Figs. 5 and 6, where the crack propagation angle θ_c and the critical failure load F_c, respectively, are plotted vs. the mixity ratio K_{II}^*/K_I^*. A general good agreement is found

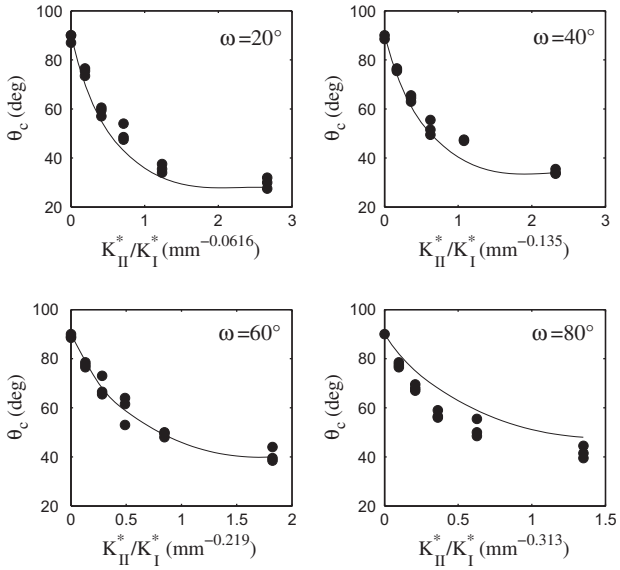

Fig. 5. Critical propagation angle θ_c vs. mixity ratio K_{II}^*/K_I^*, for different notch amplitudes ω: FFM predictions (continuous line) and experimental data on PMMA specimens [25](circles).

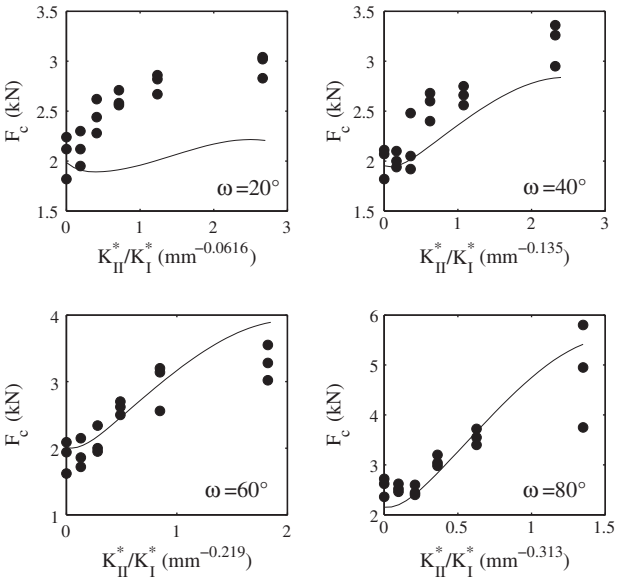

Fig. 6. Critical failure load F_c vs. mixity ratio K_{II}^*/K_I^*, for different notch amplitudes ω: FFM predictions (continuous line) and experimental data on PMMA specimens [25] (circles).

for what concerns θ_c (Fig. 5), although real values are overestimated for $\omega = 80°$, the mean deviation being nearly 9° (Table 6). The predictions on F_c match well the experimental data (typical errors being comprised in the range 0–18%), except for $\omega = 20°$, where the critical failure load results too much underestimated (Fig. 6). It should be mentioned, however, that the same occurs also for the other criteria (Table 6): this discrepacy may be due to an error related to the performed testing procedure. Indeed, for $\omega = 20°$ the best results are provided by the average stress criterion, for $\omega = 40°$ predictions by Yosibash–Leguillon criterion are the most accurate, while FFM reveals to be superior for $\omega = 60°$ and 80°.

Once again, Table 6 shows how the crack advance Δ_c becomes a structural parameter for the coupled criteria, depending on the mixity ratio as well as on the material properties.

Table 6
Averaged experimental results on PMMA samples [25] and predictions according to FFM, to Yosibash–Leguillon criterion [19] and to the average stress criterion [18].

Experimental values [25]			FFM			Yosibash–Leguillon criterion [19]			Average stress criterion [18]		
	θ_c (°)	F_c (N)	θ_c (°)	F_c (N)	Δ_c (μm)	θ_c (°)	F_c (N)	Δ_c (μm)	θ_c (°)	F_c (N)	Δ_c (μm)
$\bar{m}(\omega = 20°)$											
0.169	75	2120	70	1909	83.7	72	1922	21.3	72	1943	86.7
0.365	59	2450	55	1891	82.5	56	1930	21.9	58	1936	86.7
0.631	48	2620	43	1913	80.7	44	1981	22.4	47	1975	86.7
1.094	37	2780	34	2008	78.5	35	2106	22.8	38	2096	86.7
2.357	30	3010	28	2210	75.6	28	2347	22.9	30	2341	86.7
$\bar{m}(\omega = 40°)$											
0.127	75	2010	74	1950	83.7	77	1974	21.7	76	1983	86.7
0.275	65	2150	62	2015	82.7	64	2078	22.7	64	2058	86.7
0.476	52	2560	50	2152	81.4	53	2274	24.1	54	2210	86.7
0.824	48	2660	41	2401	79.6	42	2601	25.8	44	2485	86.7
1.776	33	3190	32	2833	76.8	33	3142	27.7	36	2963	86.7
$\bar{m}(\omega = 60°)$											
0.085	78	1910	79	2031	83.6	81	2075	22.2	81	2067	86.7
0.182	68	2010	68	2177	82.7	72	2258	23.0	72	2222	86.7
0.316	60	2610	59	2460	81.7	63	2616	24.5	62	2521	86.7
0.547	49	2970	49	2966	80.2	52	3257	27.3	53	3053	86.7
1.179	41	3280	40	3882	78.2	40	4414	31.9	42	4022	86.7
$\bar{m}(\omega = 80°)$											
0.052	75	2530	82	2199	83.1	85	2291	22.2	84	2243	86.7
0.111	65	2480	75	2408	82.4	79	2531	23.0	78	2461	86.7
0.194	55	3070	68	2836	81.7	72	3031	24.5	71	2906	86.7
0.336	50	3560	59	3663	80.6	62	4035	27.3	62	3764	86.7
0.724	40	4830	48	5414	78.8	48	6220	31.9	50	5576	86.7

Eventually, observe that, for each notch amplitude ω, the failure loads related to low mixity ratios are very close. On the other hand, FFM provides a minimum for K_{II}^*/K_I^* very small, but not null (Fig. 6), i.e. as if the minimum failure load would occur not in pure mode I, but with a small mode II contribution. On the basis of the results obtained in [31], further studies are in progress.

4. Conclusions

The coupled FFM criterion has been applied to brittle V-notched elements subjected to mixed-mode loading conditions. A good agreement with the experimental data available in the literature has generally been found. The influence of the notch root radius, which affects some results, has been discussed.

By comparing FFM results with those provided by other criteria, it can be noticed that its predictions always result the lowest ones (i.e. the most conservative), both for what concerns the critical failure load F_c and the crack propagation angle θ_c (i.e. FFM provides the highest deflections from the notch bisector). Indeed, the different theoretical estimations on F_c are very close, significant differences being observed only for higher mixity ratios. It is difficult to determine which criterion predicts better the failure initiation, changing the situation for each experimental test. For what concerns the propagation angle, FFM predictions result the most accurate in many cases.

Acknowledgements

The financial supports of the Italian Ministry of Education, University and Research (MIUR) to the Project PRIN 2008 'Advanced applications of Fracture Mechanics for the study of integrity and durability of materials and structures' and to the Project FIRB 2010 Future in Research 'Structural mechanical models for renewable energy applications' are gratefully acknowledged.

Appendix A. Stress field functions

$$f_{\theta\theta}^{I}(\theta)=\frac{1}{C_I}\{\cos[(1+\lambda_I)(\pi-\omega/2)]\cos[(1-\lambda_I)(\theta-\pi/2)]-\cos[(1-\lambda_I)(\pi-\omega/2)]\cos[(1+\lambda_I)(\theta-\pi/2)]\},\tag{A.1}$$

$$f_{r\theta}^{I}(\theta)=\frac{1}{C_I}\left\{\frac{1-\lambda_I}{1+\lambda_I}\cos[(1+\lambda_I)(\pi-\omega/2)]\sin[(1-\lambda_I)(\theta-\pi/2)]-\cos[(1-\lambda_I)(\pi-\omega/2)]\sin[(1+\lambda_I)(\theta-\pi/2)]\right\},\tag{A.2}$$

with

$$C_I=\cos[(1+\lambda_I)(\pi-\omega/2)]-\cos[(1-\lambda_I)(\pi-\omega/2)].\tag{A.3}$$

$$f_{\theta\theta}^{II}(\theta)=\frac{1}{C_{II}}\{-(1+\lambda_{II})\sin[(1-\lambda_{II})(\pi-\omega/2)]\sin[(1+\lambda_{II})(\theta-\pi/2)]+(1+\lambda_{II})\sin[(1+\lambda_{II})(\pi-\omega/2)]\sin[(1-\lambda_{II})(\theta-\pi/2)]\},\tag{A.4}$$

$$f_{r\theta}^{II}(\theta)=\frac{1}{C_{II}}\{(1+\lambda_{II})\sin[(1-\lambda_{II})(\pi-\omega/2)]\cos[(1+\lambda_{II})(\theta-\pi/2)]-(1-\lambda_{II})\sin[(1+\lambda_{II})(\pi-\omega/2)]\cos[(1-\lambda_{II})\times(\theta-\pi/2)]\},\tag{A.5}$$

with

$$C_{II}=(1+\lambda_{II})\sin[(1-\lambda_{II})(\pi-\omega/2)]-(1-\lambda_{II})\sin[(1+\lambda_{II})(\pi-\omega/2)].\tag{A.6}$$

References

[1] Neuber H. Theory of notch stress. Berlin: Springer; 1958.
[2] Ritchie RO, Knott JF, Rice JF. On the relation between critical tensile stress and fracture toughness in mild steel. J Mech Phys Solids 1973;21:395–410.
[3] Seweryn A. Brittle fracture criterion for structures with sharp notches. Engng Fract Mech 1994;47:673–81.
[4] Taylor D. Predicting the fracture strength of ceramic materials using the thoery of critical distances. Engng Fract Mech 2004;71:2407–16.
[5] Lazzarin P, Zambardi R. A finite-volume-energy based approach to predict the static and fatigue behavior of components with sharp V-shaped notches. Int J Fract 2001;112:275–98.
[6] Pugno N, Ruoff R. Quantized fracture mechanics. Philos Mag 2004;84:2829–45.
[7] Yosibash Z, Bussiba A, Gilad I. Failure criteria for brittle elastic materials. Int J Fract 2004;125:307–33.
[8] Taylor D, Cornetti P, Pugno N. The fracture mechanics of finite crack extension. Engng Fract Mech 2005;72:1021–38.
[9] Cornetti P, Pugno N, Carpinteri A, Taylor D. Finite fracture mechanics: a coupled stress and energy failure criterion. Engng Fract Mech 2006;73:2021–33.

[10] Leguillon D. Strength or toughness? A criterion for crack onset at a notch. Eur J Mech A/Solids 2002;21:61–72.
[11] Carpinteri A, Cornetti P, Pugno N, Sapora A, Taylor D. A finite fracture mechanics approach to structures with sharp V-notches. Engng Fract Mech 2008;75:1736–52.
[12] Carpinteri A, Cornetti P, Pugno N, Sapora A, Taylor D. Generalized fracture toughness for specimens with re-entrant corners: experiments vs. theoretical predictions. Struct Eng Mech 2009;32:609–20.
[13] Leguillon D, Yosibash Z. Crack onset at a V-notch: influence of the notch tip radius. Int J Fract 2003;122:1–21.
[14] Picard D, Leguillon D, Putot C. A method to estimate the influence of the notch-root radius on the fracture toughness of ceramics. J Eur Ceram Soc 2006;26:1421–7.
[15] Carpinteri A, Cornetti P, Sapora A. Brittle failures at rounded V-notches: a finite fracture mechanics approach. Int J Fract 2011;172:1–8.
[16] Carpinteri A, Cornetti P, Sapora A. A finite fracture mechanics approach to the asymptotic behaviour of U-notched structures. Fatigue Fract Engng Mater Struct 2012;35:451–7.
[17] Sih GC. Strain-energy-density factor applied to mixed mode crack problems. Int J Fract 1974;10:305–21.
[18] Seweryn A, Mroz Z. A non-local stress failure condition for structural elements under multiaxial loading. Engng Fract Mech 1995;51:955–73.
[19] Yosibash Z, Priel E, Leguillon D. A failure criterion for brittle elastic materials uder mixed-mode loading. Int J Fract 2006;141:291–312.
[20] Seweryn A, Lukaszewicz A. Verification of brittle fracture criteria for elements with V-shaped notches. Engng Fract Mech 2002;69:1487–510.
[21] Priel E, Bussiba A, Gilad I, Yosibash Z. Mixed mode failure criteria for brittle elastic V-notched structures. Int J Fract 2007;144:247–65.
[22] Gomez FJ, Elices M, Berto F, Lazzarin P. Fracture of V-notched specimens under mixed mode (I + II) loading in brittle materials. Int J Fract 2009;159:121–35.
[23] Williams ML. Stress singularities resulting from various boundary conditions in angular corners of plate in extension. J Appl Mech 1952;19:526–8.
[24] Beghini M, Bertini L, Di Lello R, Fontanari V. A general weight function for inclined cracks at sharp V-notches. Engng Fract Mech 2007;74:602–11.
[25] Seweryn A, Poskrobko S, Mroz Z. Brittle fracture in plane elements with sharp notches under mixed-mode loading. J Engng Mech 1997;123:535–43.
[26] Hills DA, Dini D. Characteristics of the process zone at sharp notch roots. Int J Solids Struct 2011;48:2177–83.
[27] Carpinteri A. Stress-singularity and generalized fracture toughness at the vertex of re-entrant corners. Engng Fract Mech 1987;26:143–55.
[28] Hasebe N, Iida J. A crack originating from a triangular notch on a rim of a semi-infinite plate. Engng Fract Mech 1978;10:773–82.
[29] Philipps AG, Karuppanan S, Churchman CM, Hills DA. Crack tip stress intensity factors for a crack emanating from a sharp notch. Engng Fract Mech 2008;75:5134–9.
[30] Priel E, Yosibash Z, Leguillon D. Failure initiation at a blunt V-notch tip under mixed mode loading. Int J Fract 2008;149:143–73.
[31] Carpinteri A, Cornetti P, Pugno N, Sapora A. On the most dangerous V-notch. Int J Solids Struct 2010;47:887–93.